Astronomy & Astrophysics manuscript no. output
July 14, 2023

Characterizing the features of the low-amplitude peaks in delta Scuti stars with TESS

S. Barceló Forteza[1], J. Pascual-Granado[2], J. C. Suárez[1], A. García Hernández[1], G. M. Mirouh[1], and M. Lares-Martiz[2]

[1] Física Teórica y del Cosmos Dept., Universidad de Granada (UGR), 18071, Granada, Spain
[2] Instituto de Astrofísica de Andalucía (CSIC), Glorieta de la Astronomía s/n, 18008, Granada, Spain

Received XX Month 20YY; Accepted ZZ Month 20YY

ABSTRACT

The presence of low-amplitude peaks, often referred to as "*grass*", in the power spectra of δ Scuti stars is frequently disregarded. However, these seemingly insignificant peaks might contain valuable information about the origin of these stars and the reasons behind the occurrence or absence of a flat plateau. It is crucial to systematically parameterize the grass phenomenon across a comprehensive sample that covers the entire δ Scuti star range on the HR Diagram. By doing so, we can conduct a quantitative investigation of this phenomenon, leading to improved detection methods for flat plateaus and a deeper understanding of their nature.
To address these objectives, we leveraged long-duration, high-duty-cycle TESS light curves of δ Scuti stars. This approach minimizes the impact of unresolved peaks caused by mode variations over time. Additionally, we employed appropriate analysis techniques to mitigate window effects and identify and eliminate spurious peaks.
We demonstrate here that the grass can be effectively parameterized based on peak density. With such parameterization two distinct regimes were found: the "*sparse grass regime*", characterized by low grass density and the absence of a flat plateau in the power spectra, and the "*dense grass regime*", characterized by high grass densities and the presence of an observable flat plateau.
Our study is the first rigorous quantification of the emergence of a plateau in the power spectra of δ Scuti stars. The parameterization of the grass properties opens the way to the study of fractality, mode variability, and rotation.

Key words. asteroseismology - stars: oscillations - stars: variables: δ Scuti

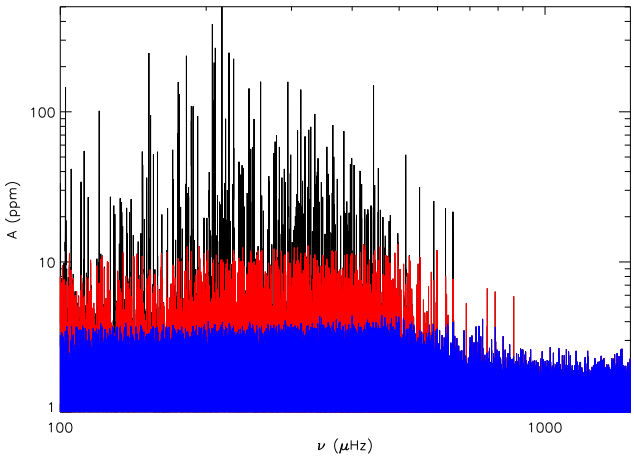

Fig. 1. Power spectrum of TIC 198456033, a δ Scuti star with flat plateau (black). Red points to the contribution of grass peaks. Blue represents the power spectrum below detection limit.

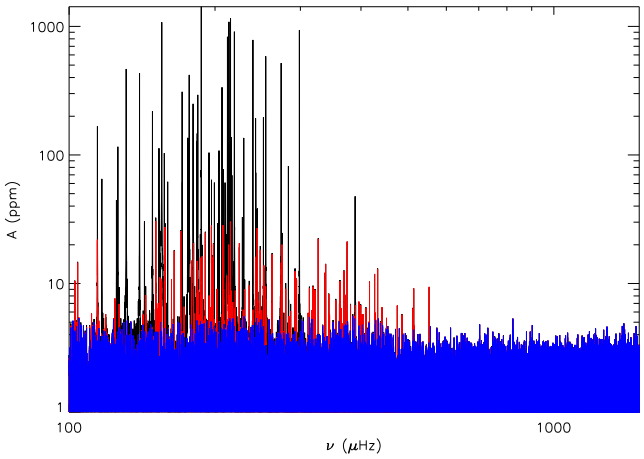

Fig. 2. Same as Fig. 1 but for TIC 232604221, a δ Scuti star without flat plateau.

1. Introduction

The classical stellar pulsators known as δ Scuti stars are A-F intermediate mass stars (1.5 to 2.5 $M_{\odot}$; Breger 2000) with temperatures from 6000 to 9000 K (Uytterhoeven et al. 2011) and frequencies between 50 and 930 μHz. Their main excitation mechanism is known as the κ-mechanism (Chevalier 1971) although other mechanisms may play a significant role (Antoci et al. 2014; Xiong et al. 2016).

Some of the first δ Scuti stars observed by CoRoT space telescope (Baglin et al. 2006) present a flat power excess unobservable from the ground, made by a high number of low-amplitude peaks, that sharply decreases at higher frequencies down to noise (Poretti et al. 2009). Fig. 1 shows the power spectrum of a δ Scuti star with flat plateau. The amplitudes of the peaks are slightly

higher than the background noise, but they are still statistically significant.

There are many possible (non-)physical phenomena behind the origin of this power-spectral feature. For example, the flat plateau may be produced by a cascade bug during the analysis of the data (Balona 2014) or by the possible non-harmonic nature of the observed power spectra (Pascual-Granado et al. 2015).

Split peaks due to mode variations in time are commonly observed since ∼ 45% of the power spectra of Kepler δ Scuti stars have one sidelobe (Balona & Dziembowski 2011). This is in agreement with Barceló Forteza et al. (2020) where it is shown how 73% of δ Scuti stars of their ∼2300 star sample present different kinds of split peaks. Each kind may be explained with different mechanisms. These mechanisms can be extrinsic to the modes, such as orbital Doppler effect in multiple systems (Shibahashi & Kurtz 2012); or intrinsic, such as mode coupling (e.g., Moskalik 1985; Buchler et al. 1997; Barceló Forteza et al. 2015).

A possible explanation could be a granulation background signal that may develop in cool δ Scuti stars since they could have thin outer convective layers (Kallinger & Matthews 2010; Balona 2011). Another cause may be a misaligned magnetic field from the rotation axis that splits the modes into $(2l + 1)^2$ peaks (Goode & Thompson 1992). However, it may not be common in δ Scuti stars since only a few detections have been reported (Kurtz et al. 2008; Neiner et al. 2017; Zwintz et al. 2020).

Rotation is one of the most plausible mechanisms. A high rotation rate modifies the shape of the star from a sphere to an oblate spheroid. Owing to the geometry of the star, a less-effective disc-averaging of the flux allows to observe higher degree modes than the spherical case (up to l=20, Kennelly et al. 1998; Poretti et al. 2009). In addition, the oblateness of the star can lead to the emergence of a significant number of chaotic modes (Lignières & Georgeot 2009). Not only fast rotation is widespread in A-type stars (e.g. Royer et al. 2007), but also it is related to many of the other phenomena, such as the magnetic fields or the rotational mode coupling.

Each of these physical mechanisms may be of different importance depending on the particular characteristics of each δ Scuti star. In fact, Barceló Forteza et al. (2017, BF2017 hereafter) contends that the two main mechanisms are rotation and mode variation.

To study the low-amplitude peaks of the power spectra, BF2017 defined the so-called grass as the low-amplitude peaks within δ Scuti frequency regime with $S_i \lesssim 0.01\%$ where

$$S_i(\%) \equiv 100 \frac{(rms_i - rms_{i+1})}{rms_0}, \quad (1)$$

and rms_i is the root mean square of the residual signal before subtracting the i-th peak from the pulsation signature assuming a flux given by

$$F \approx \sum_i A_i \sin(2\pi\nu_i t + \phi_i) + N, \quad (2)$$

in which each harmonic signature is characterized by its frequency, amplitude, and phase (ν_i, A_i, ϕ_i, respectively), and N is the background noise. Then, S_i is the contribution of the peak to the entire light curve. Taking into account its definition, grass peaks may or may not form a plateau. Fig. 1 highlights the dense contribution of the grass to the flat plateau down to the detection limit. On the contrary, Fig. 2 shows a few scattered grass peaks but no plateau.

This S_i limit is useful to differentiate the grass peaks from these of the envelope with higher amplitudes. The envelope peaks origin is mainly pulsation and they follow several scaling relations such as the low-order large separation - mean density of the star (Suárez et al. 2014; García Hernández et al. 2015; García Hernández et al. 2017; Bedding et al. 2020), and the temperature, gravity and frequency at maximum power (e.g., Balona & Dziembowski 2011; Moya et al. 2017; Barceló Forteza et al. 2018; Bowman & Kurtz 2018; Barceló Forteza et al. 2020; Hasanzadeh et al. 2021). BF2017 defined the envelope as the peaks within the δ Scuti pulsation regime with $S_i \gtrsim 0.1\%$. The peaks between the upper limit of the grass regime ($S_i \lesssim 0.01\%$) and the envelope lower limit may belong to one of these two regimes. They used these different limits to avoid using peaks belonging to the other region that might influence the results. In this work, we will follow these definitions.

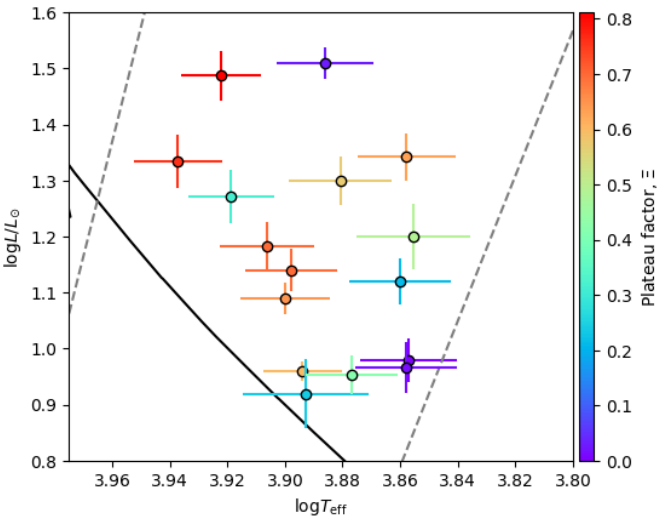

Fig. 3. Sample of δ Scuti stars from TESS Cycle 2. Redder colors indicate the presence of a flat plateau. The black line points to the Zero Age Main Sequence. Grey dashed lines represent red and blue limits of the instability strip for observed pulsators in the δ Scuti regime (Murphy et al. 2019).

BF2017 studied the grass of four δ Scuti stars in order to unveil the characteristics of the flat plateau. Using the power spectra of the residual light curve after subtracting the envelope, they calculated the mean amplitude of the grass (A_g), and the mean density of peaks ($\bar{n}$; see Fig. 6 and 7 in BF2017). To calculate these values, they take into account the typical frequency regime of δ Scuti pulsations up to the cut-off frequency, ν_c, where the amplitude/density of peaks significantly decay.

Here, we present a quantitative study of the flat plateau phenomenon that allow its parameterization, improving the understanding of its nature and how it is detected. In Sect. 2, we introduce our sample of δ Scuti stars in order to cover the most representative cases. We explain how data is analyzed including low-duty-cycle light curve reduction and how its power spectral structure is classified via their signal (S_i, see Sect. 3). In addition to the characterization laid out by BF2017, we propose the plateau factor, i.e., the steadiness of the amplitude across the plateau, obtaining two different regimes (see Sect. 4). Taking into account our results, we discuss the possible mechanisms behind the emergence of the flat plateau in Sect. 5. Finally, we present our conclusions in Sect. 6.

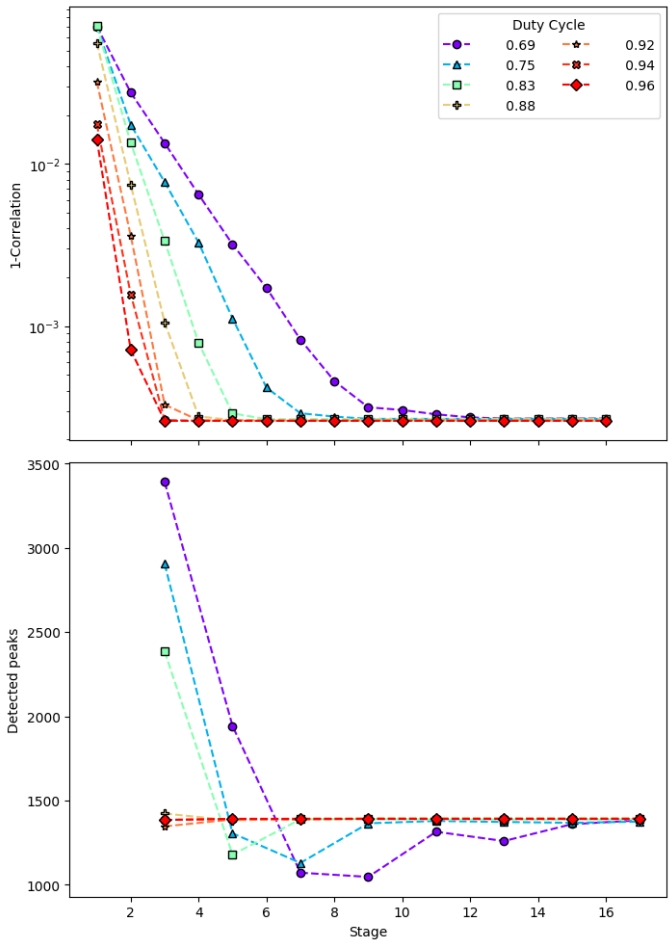

Fig. 4. Top panel: Deviation from perfect correlation at each stage between the original and detected harmonic flux for high-quality data points for simulated δ Scuti light curves with different realistic duty cycles. Bottom panel: Number of detected peaks as a function of the number of stages for the same simulations as above panel.

2. Data from space telescopes

We study the light curves of our sample of stars representative of the δ Scuti frequency regime. Fig. 3 presents the Hertzsprung-Russel diagram location of the stars in our sample inside the instability strip. They are color-coded by the plateau factor we will introduce in Sect. 4.

The high photometric precision required to study peaks of a few parts-per-million is reached by space telescopes such as CoRoT, or Kepler (Baglin et al. 2006; Borucki et al. 2010). The longer the campaign, the better to avoid unresolved peaks of the power spectrum due to mode variations (BF2017). For example, the four-year-long observations of Kepler allow us to observe cyclic variations of some δ Scuti star modes with periods up to years (e.g., Barceló Forteza et al. 2015). Nevertheless, Kepler long cadence (~30 min) produces power spectra with lower Nyquist frequency ($\nu_{Ny} \sim 283\,\mu$Hz) than the highest frequencies of the typical pulsation regime for δ Scuti stars. These datasets can be used to study high-amplitude peaks via superNyquist asteroseismology (Murphy et al. 2013), but not for very dense spectra saturated with low-amplitude frequency-blended peaks.

Then, we selected a homogeneous sample only from *TESS* (Transiting Exoplanet Survey Satellite; Ricker et al. 2015) using all Cycle 2 sectors. These stars are from, or close to, the southern pole continuous viewing zone. This yields a ~352-day light curve and a Rayleigh frequency of 33nHz. The cadence of the studied *TESS* light curves is ~2 minutes. Therefore, the Nyquist frequency is 4167 μHz, covering, by far, all the typical frequency regime. Using all available sectors, their duty cycle range between 76% to 85% due to periodic data downlinks and several data anomalies.

After their reduction (see Sect. 3), we provide the first analysis of sixteen previously unstudied TESS light curves (Table O.1 to O.16 available online).

3. Methodology

We employed the δ Scuti Basics Finder pipeline (referred to as δSBF hereafter, see BF2017 and references therein) to characterize the power-spectral structure of this particular type of stars. The pipeline's three-stage method, consisting of two independent interpolation stages and one frequency analysis stage (see Barceló Forteza et al. 2015, for detailed information), allowed us to effectively fill the gaps in the light curves by utilizing information from the previously subtracted peaks.

During each prewhitening step, we calculated S_i, and promptly identified any spurious peaks, signaling the completion of that stage. Spurious peaks exhibit a negative signal, as they contribute harmonically instead of being subtracted ($S_i < 0$, see Eq. 1). This alarm serves to notify us that spurious peaks can only arise due to slight variations between the original data and the filled gaps, which are considered authentic solely during the analysis stage. To be considered valid, all detected peaks must have a signal-to-noise ratio of 4 or higher.

The three-stage method effectively minimizes the impact of gaps and significantly reduces background noise. It can reduce background noise by up to a factor of 3 for duty cycles of 60% and up to 14 for duty cycles around 90% (Barceló Forteza et al. 2020). The efficacy of gap-filling improves with each interpolation stage, benefiting from the availability of more information in the light curve. This improvement stems from the minimization of errors in the subtracted harmonic parameters after each stage. Furthermore, the method's efficiency is augmented by the excellent observational window provided by space missions and the high signal-to-noise ratio (García et al. 2014; Barceló Forteza et al. 2015).

To further enhance the detection of spurious peaks resulting from slight differences between real data and interpolation, we introduce here the 2K+1 stage method, an upgraded procedure involving 2K independent interpolation stages and a final frequency analysis stage.

We validated our procedure by conducting tests using simulated light curves containing approximately 1400 actual δ Scuti star oscillations. These tests incorporated elements such as noise, realistic TESS duty cycles, and the presence of gaps. The top panel of Figure 4 illustrates the deviation from the harmonic model (see Eq. 2 with $N = 0$) for the high-quality data in the simulated light curves, excluding the points identified as gaps. In all cases, the deviation from the harmonic model decreases until reaching a minimum value, distinct from 0 due to the presence of simulated noise. The bottom panel depicts the number of detected peaks after the 2K+1 stages. Our results demonstrate that three stages are sufficient for analyzing low-amplitude peaks in light curves with high duty cycles ($\gtrsim$90%). In these light curves, the appropriate number of peaks is detected, and the deviation from the harmonic model reaches its minimum at the third stage. For lower duty cycles, additional stages are required to avoid spurious peaks and accurately detect the genuine ones.

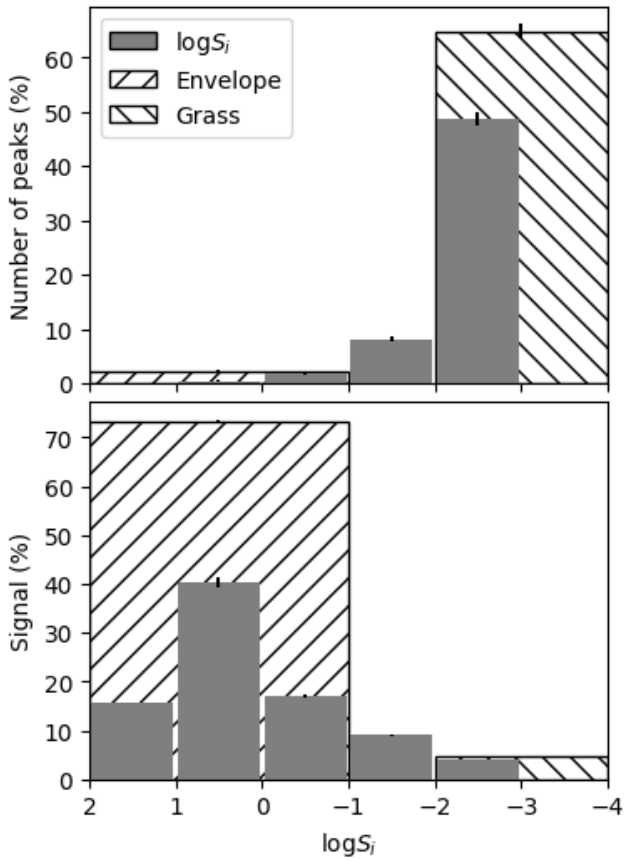

Fig. 5. Top panel: Contribution to the number of peaks subtracted from TIC 198456033 power spectrum as a function of their signal level. Note the error bars on top of each measurement. Bottom panel: Same as top panel for the contribution to the total amount of signal.

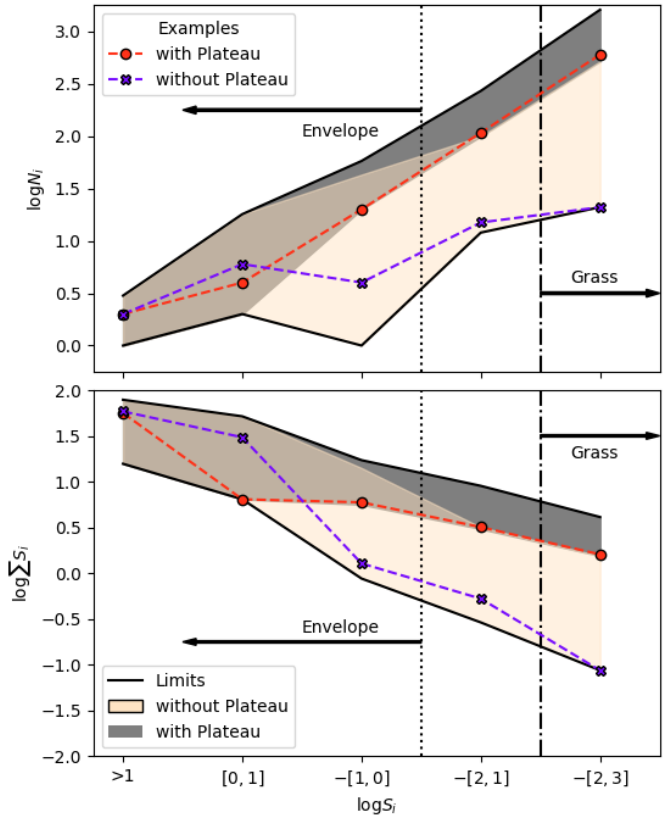

Fig. 6. Top panel: Typical number of peaks subtracted from the power spectra for our sample of δ Scuti star at each signal level (from top to bottom solid black lines). Grey and beige areas point to the typical values for cases with and without flat plateau, respectively. We also included two representative cases (red circles and purple x dashed lines, respectively). Bottom panel: Same as the top panel but for the contribution to the total amount of signal.

In studying our sample of stars, we determine the optimal number of stages that minimize their deviation from the harmonic model. We also consider the minimum stages required based on their duty cycles, as determined through simulations. For these reasons, the required stages to reduce the light curves we consider here are a minimum of seven.

3.1. Signal analysis

After the frequency analysis of each δ Scuti star, we studied the number of peaks and their contribution to the total amount of signal taking into account their signal level ($\log S_i$, see Fig. 5 for an example). We focus on peaks from the envelope ($\log S_i \geq -1$) and those belonging to the grass ($\log S_i \leq -2$). On the one hand, the power spectrum presents a considerably higher percentage of grass peaks than those from the envelope (see top panel in Fig. 5). On the other hand, the contribution to the signal of a single dominant peak ($\log S_i \geq 1$; see bottom panel) is several times bigger than all peaks from grass: a ∼15% compared to a ∼5% for this particular star.

However, the number of peaks of each regime and their contribution to the signal are different for each star. Fig. 6 shows the typical values of both parameters for the stars of our sample. We differentiated the stars with and without plateau (grey and beige areas, respectively). The envelope shows no separation between both kinds of power spectra. On the contrary, they are well separated in the grass. We also compared two specific δ Scuti stars with (TIC 230136491; red line) and without a plateau (TIC 259130275; purple line). Both have a similar number of dominant peaks and contribution to the signal but they differ by orders of magnitude at grass level.

4. Grass parameterization

As in BF2017, we also use δSBF to parameterize the grass by studying the mean amplitude and the mean density of peaks per 10-μHz bin ($A_{\rm bin}$ and $n_{\rm bin}$, see top and bottom panels of Fig. 7, respectively). However, we modify the pipeline in order to characterize and compare all kinds of δ Scuti stars, including hybrids, only measuring their grass properties in the δ Scuti frequency regime (see Sect. 1). Instead of using the rough limit between γ Doradus and δ Scuti frequency regimes at ∼50μHz, we calculate the frequency at minimum peak density (ν_λ) around the fundamental mode. The density of peaks for δ Scuti stars shows a minimum between g and p modes domain (Moya et al. 2017, ; see also bottom panels in Fig. 7).

We also modified the way we calculate the cut-off frequency. Fig. 7 presents two characteristic cases of grass with and without plateau (TIC 198456033 and TIC 232604221, as in Fig. 1 and 2, respectively). The left column shows a grass with flat plateau. As we described in Sect. 1, in this case the grass manifests a high density of peaks with stable amplitude at frequencies up to the cut-off frequency. For higher frequency peaks up to the higher

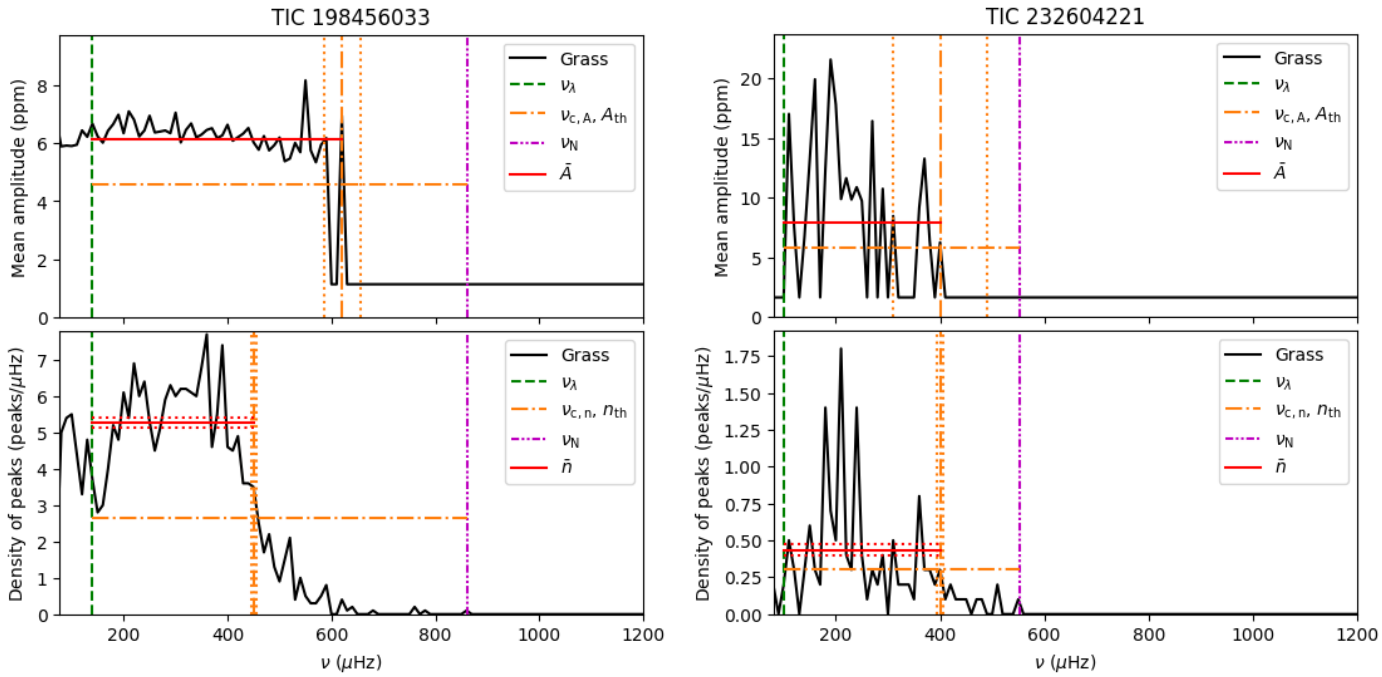

Fig. 7. Grass parametrization for TIC 198456033 and TIC 232604221 (left and right columns, respectively). Top panels: Mean amplitude of grass peaks per 10-μHz bin (black solid) compared with the mean amplitude of the plateau ($\bar{A}$; red solid) from the frequency at minimum peak density (ν_λ; green dashed) to the cut-off frequency for amplitude ($\nu_{c,A}$; dashed-dotted orange). The amplitude threshold is also represented (A_{th}; dashed-dotted orange). Bottom panels: Mean density of grass peaks per 10-μHz bin (black solid) and the mean density of grass peaks ($\bar{n}$; red solid) between the frequency at minimum peak density (dashed green) and the cut-off frequency for peak density ($\nu_{c,n}$; dashed-dotted orange). The density threshold is also represented (n_{th}; dashed-dotted orange).

frequency detected (ν_N), the density of peaks rapidly decreases and their amplitude drops to noise. On the contrary, right column in Fig. 7 shows a grass without plateau, i.e., a low density of grass peaks and an unstable amplitude, including empty bins with no peaks. The grass density decrease after the cut-off frequency is barely noticeable.

Then, to constrain the plateau frequency regime, we measure the cut-off frequency for peak density ($\nu_{c,n}$). At that frequency, the mean density of peaks per bin ($n_{\rm bin}$) decrease below the following threshold,

$$n_{th} = N^{-1}_{\rm bins}(\nu_\lambda, \nu_N) \sum_{\nu_\lambda}^{\nu_N} n_{\rm bin}(\nu) \approx n_g \,, \tag{3}$$

where n_g is the mean density of grass peaks for all the δ Scuti frequency regime; and $N(\nu_a, \nu_b)$ is the number of bins between the frequencies. Finally, we measure the mean density of the plateau ($\bar{n}$) using its proper limits,

$$\bar{n} = N^{-1}_{\rm bins}(\nu_\lambda, \nu_{c,n}) \sum_{\nu_\lambda}^{\nu_{c,n}} n_{\rm bin}(\nu) \,. \tag{4}$$

We have taken a similar approach studying the amplitudes. The cut-off frequency for amplitude ($\nu_{c,A}$) points to the decay of the mean amplitude per bin ($A_{\rm bin}$) below their threshold (A_{th}; analogously to Eq.. 3). Since the density of peaks and the amplitude do not have to reach their threshold value at the same frequency, the two cut-off frequencies do not have to be equal (see right panels in Fig. 7). Then, the mean amplitude of the plateau is

$$\bar{A} = N^{-1}_{\rm bins}(\nu_\lambda, \nu_{c,A}) \sum_{\nu_\lambda}^{\nu_{c,A}} A_{\rm bin}(\nu) \,. \tag{5}$$

The stability of the mean amplitude can be used to study the presence or absence of a flat plateau. Then, we define the plateau factor as

$$\Xi \equiv 1 - N^{-1}_{\rm bins}(\nu_\lambda, \nu_{c,n}) \sum_{\nu_\lambda}^{\nu_{c,n}} \left| 1 - \frac{A_{\rm bin}(\nu)}{\bar{A}} \right| \,, \tag{6}$$

The higher the plateau factor, the more similar is the grass to a boxcar function. We also visually note this relation by comparing the power spectra for the two stars discussed previously with high and low plateau factors (left and right columns in Fig. 8, respectively). Each panel of Fig. 8 shows the power spectral structure of the original light curve, and also after subtracting a consecutive signal level down to the detection limit. These two stars have a similar number of peaks in the envelope but TIC 198456033 has one order of magnitude more peaks in the grass forming the plateau (see second panels from bottom). In addition to the sparse grass peaks of TIC 232604221, their amplitudes are far from stable. Moreover, TIC 198456033 presents a power excess in the δ Scuti frequency regime at the detection limit compared with noise (see bottom panel of Fig. 8). On the contrary, TIC 232604221 lacks of this power excess once the detection limit is reached.

We repeat this exercise for all stars of our sample. Taking into account the peaks at each signal level, Fig. 9 shows a random distribution regarding the presence of flat plateau ($\Xi \to 1$) at each signal level of the envelope. Nevertheless, this distribution is organized between signal levels $-1 \geq \log S_i \geq -2$ and remains down to the detection limit. The higher the grass contribution, the higher the plateau factor. In fact, all cases with $\Xi \gtrsim 0.64$ show a grass with flat plateau (grey area in Fig. 9). This distribution suggests that the limits between grass and envelope properly

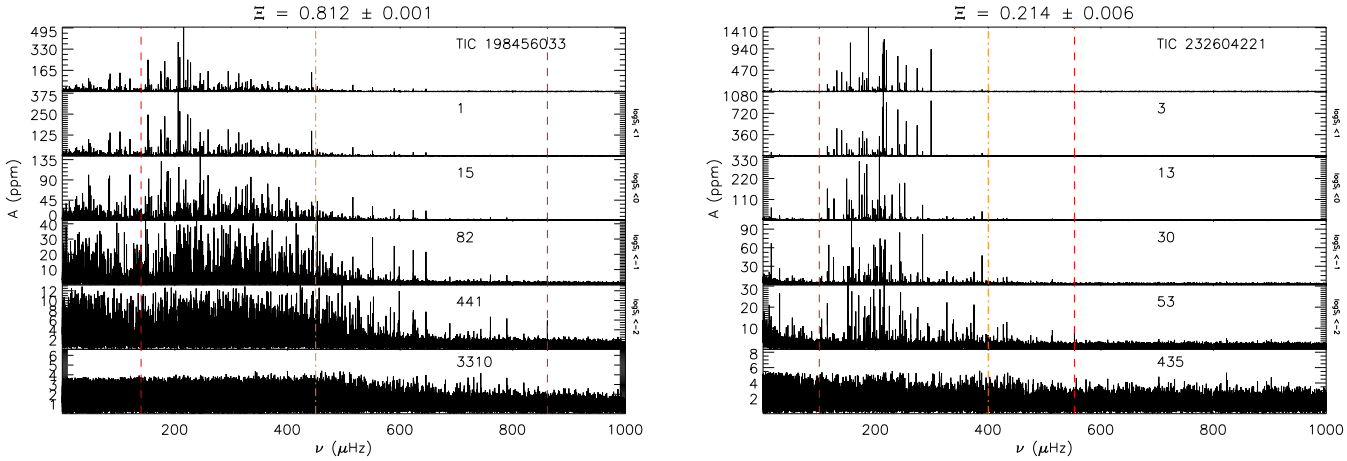

Fig. 8. From top to bottom: Power-spectral structure of the original light curve for TIC 198456033 (left column) and TIC 232604221 (right column), and also those after extracting the indicated number of peaks. The second panel from the bottom shows the grass level and the presence or absence of a flat plateau (Ξ, see text). Red dashed lines point to ν_λ and the highest detected frequency (ν_N). Orange dashed-dotted line points to the cut-off frequency ($\nu_{c,n}$).

separate both power spectral structures and the mechanisms for the plateau emergence should be further explored.

4.1. With(out) flat plateau

The definition of the plateau factor is not related with the density of grass peaks but with their mean amplitude throughout the pulsation regime. However, we find that the higher the mean density of peaks, the higher the plateau factor (see Fig. 10). In fact, we can differentiate two grass regimes,

$$\Xi = \begin{cases} (0.53 \pm 0.18)\bar{n} - (0.04 \pm 0.09), & \bar{n} \lesssim 1.03 \pm 0.12 \\ (48 \pm 6)10^{-3}\bar{n} + (0.55 \pm 0.02), & \bar{n} \gtrsim 1.03 \pm 0.12\,; \end{cases} \quad (7)$$

where the Pearson correlation coefficient for each regime is r∼0.823 and r∼0.961, respectively. For the sparse grass regime, the plateau factor rapidly increases with $\bar{n}$ up to a saturation limit ($\Xi_s \sim 0.60 \pm 0.02$). On the contrary, the dense grass regime slightly increases with $\bar{n}$. This limit is in agreement with the observed flat plateau for all δ Scuti stars with $\Xi \gtrsim 0.64$ (see Fig. 9).

The grass density decay,

$$\Delta n = \bar{n} - n_g\,, \quad (8)$$

also presents these two regimes (see Fig. 11). For power spectra at the sparse grass regime ($\Xi \lesssim 0.6$), the grass density decay is close to zero. On the contrary, the decay significantly increases after the saturation limit,

$$\Delta n = \begin{cases} 0.19 \pm 0.13, & \Xi \lesssim 0.60 \pm 0.02\,; \\ (12.6 \pm 2.3)\Xi + (7.3 \pm 1.1), & \Xi \gtrsim 0.60 \pm 0.02\,; \end{cases} \quad (9)$$

where r∼0.964. δ Scuti stars at the dense grass regime ($\Xi \gtrsim 0.6$) show a significantly higher density of grass peaks within the frequency regime $\nu \in [\nu_\lambda, \nu_{c,n}]$ than outside.

Regarding the amplitudes, Fig. 12 shows how the plateau mean amplitude distribution appears to be completely random. The signal-to-noise ratio of the low-amplitude structure is around 5 or higher for all cases except for two δ Scuti stars at the sparse grass regime. Therefore, most of them can be considered as significant structures. Nevertheless, these structures in

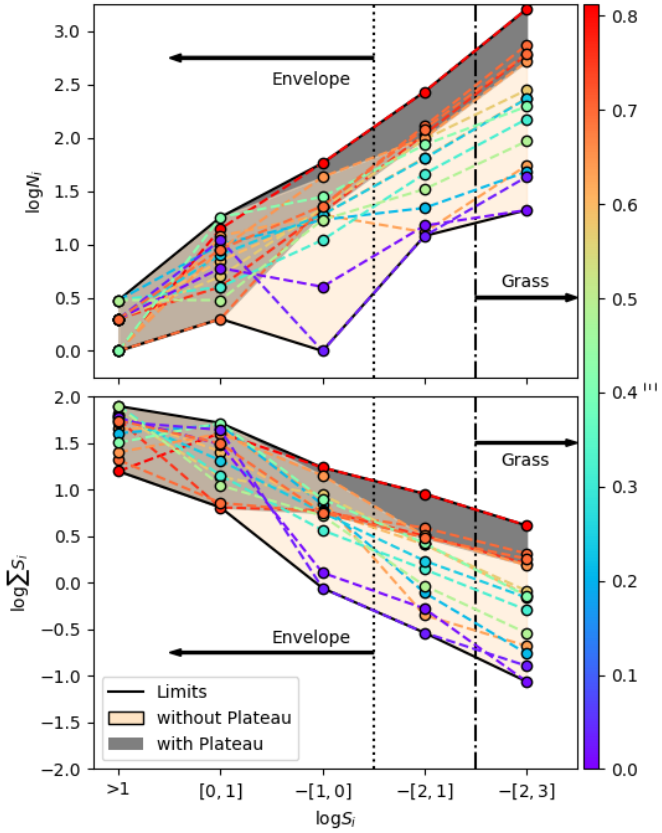

Fig. 9. Top panel: Number of peaks subtracted from the power spectrum of each δ Scuti star with regard to their signal level. Bottom panel: Same as the top panel for the contribution to the total amount of signal. Redder colors indicate a higher plateau factor (Ξ, see Sect. 4). As in Fig. 6, the grey (beige) area indicates a grass with(out) flat plateau.

the sparse grass regime cannot be called plateau, they are only a dispersed significant peaks.

Finally, our results, compiled in Table 1, are in agreement with the qualitative study of the low-amplitude part of the power spectra for δ Scuti stars: there are stars with and without flat

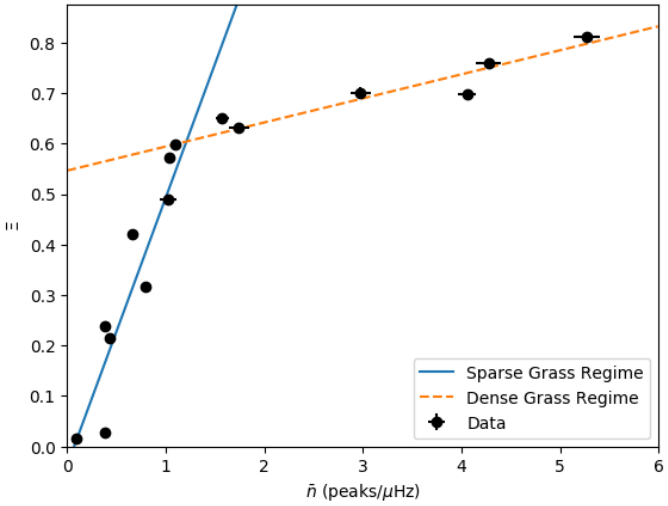

Fig. 10. Plateau factor with the mean density of grass peaks (black points). The plateau factor follows two different relations depending on the regime: the sparse grass regime (solid blue line) and the dense grass regime (dashed orange line).

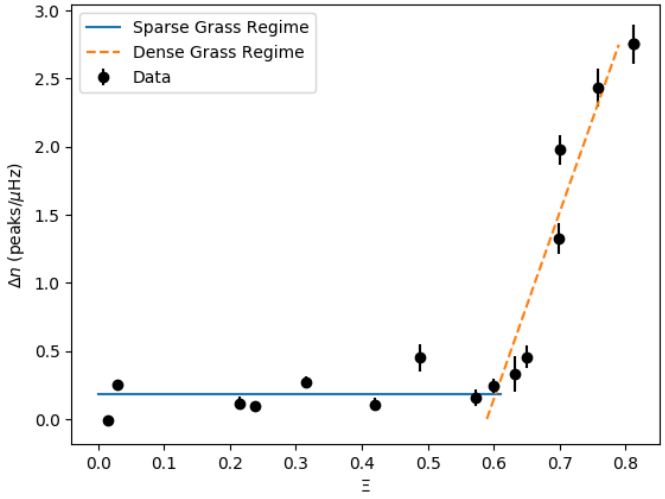

Fig. 11. Grass density decay versus the plateau factor. Solid blue (dashed orange) line represents the relation between both parameters at sparse (dense) grass regime.

plateau. The plateau factor allows us to quantitatively characterize the power spectra but separates these two regimes thanks to its saturation value: $\Xi_s \sim 0.60 \pm 0.02$. The power spectra at the sparse grass regime do not have enough density of grass peaks to create a flat plateau. But power spectra at the dense grass regime have a high density of peaks, with a significant decay towards high frequencies, allowing us to observe the plateau.

5. Discussion

After having characterized the behaviour of the low-amplitude power spectra of δ Scuti stars, studying the differences between members belonging to each regime may help us to find the mechanism for the emergence of the flat plateau.

At this point, we can rule out the possibility of a cascade bug as the main cause of the flat plateau. An important key point is the windows effect correction. Low-duty-cycle light curves should be properly interpolated or the low-amplitude

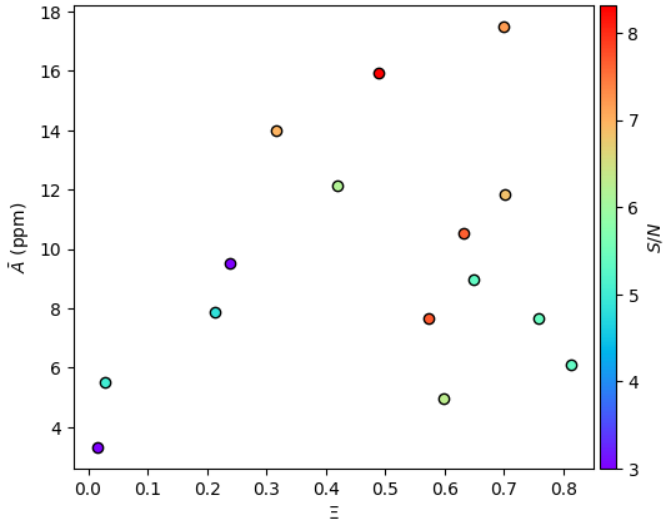

Fig. 12. Mean amplitude of the plateau versus the plateau factor. The color points to the signal-to-noise ratio.

peaks should not be studied (see Fig. 4). Using our methodology, we recover non-spurious peaks only ($S_i > 0$). Moreover, we noted that TIC 198456033 and TIC 232604221 have the same duty cycle (83.8%) but they are cases of power spectra with and without flat plateau, respectively. However, the higher number of peaks, the higher number of errors should produce the prewhitening method (Balona 2014). The typical number of genuine peaks of the envelope is around a few tens (Barceló Forteza et al. 2018). This is in agreement with number of envelope peaks for our sample for any Ξ ($\log N_i \sim 1.5$, see Fig. 9). Since there is no relation between the number of envelope peaks and the presence of a flat plateau, a cascade bug due to consecutive errors in the analysis should not be the main cause of the presence of a flat plateau. Oppositely, the non-harmonic nature of the signal referred by Pascual-Granado et al. (2015) and Suárez et al. (2020) might originate non-spurious peaks so fractality cannot be discarded as a plausible cause for the flat plateau.

The maximum density of peaks reached in our sample ($n_{\max} \sim 9.6 \pm 0.4$ peaks/μHz) implies one peak each 100 nHz, approximately three times the Rayleigh frequency of our light curves ($\nu_R \sim 33$ nHz). Although this is not a guarantee for the absence of unresolved peaks due to period or amplitude variations, their presence has been minimized thanks to our strategy (see Sect. 2). δ Scuti stars may have cyclic variations from months to years (e.g., Barceló Forteza et al. 2015; Bowman et al. 2016) and the stars of our sample are not an exception (Barceló Forteza et al., in prep.). BF2017 suggests mode variation as one of the main causes of the presence of the flat plateau apart from rotation. In fact, both phenomena may be related via rotational mode coupling (Buchler et al. 1995).

5.1. Down to the background

The statistical model used to estimate the background noise and, therefore, the detection of significant peaks in the power spectrum, depend on hypotheses about the physical properties of the star. Noise may not only include the non-frequency dependent white noise but other components such as those produced by activity or granulation (Harvey 1985). The observation of this stochastic motion requires a convective surface such as in Sun-like stars (Michel et al. 2008) and red giants (Kallinger

$T_{\rm eff}$ (K)	L ($L_\odot$)	ν_λ (μHz)	$\nu_{\rm c,n}$ (μHz)	$\nu_{\rm N}$ (μHz)	$\bar{A}$ (ppm)	Ξ	$\bar{n}$ (peaks/μHz)	Δn (peaks/μHz)	Grass Regime
8360 ± 120	30.7 ± 1.4	140 ± 5	450 ± 5	861.473	6.11 ± 0.15	0.812 ± 0.001	5.27 ± 0.13	2.75 ± 0.14	Dense
7200 ± 120	9.5 ± 0.4	100 ± 10	-	180.973	-	-	-	-	No grass detected
7210 ± 120	22.0 ± 0.9	70 ± 5	240 ± 5	307.561	10.5 ± 0.4	0.632 ± 0.003	1.74 ± 0.10	0.33 ± 0.13	Dense
8650 ± 130	21.5 ± 1.0	140 ± 5	400 ± 5	792.089	7.7 ± 0.4	0.758 ± 0.001	4.27 ± 0.13	2.43 ± 0.14	Dense
7250 ± 130	13.2 ± 0.6	100 ± 5	400 ± 5	553.060	7.9 ± 1.1	0.214 ± 0.006	0.43 ± 0.04	0.12 ± 0.05	Sparse
7830 ± 110	9.11 ± 0.16	140 ± 5	690 ± 5	916.651	4.96 ± 0.26	0.599 ± 0.002	1.10 ± 0.05	0.24 ± 0.06	Saturation point
7910 ± 130	13.8 ± 0.5	160 ± 10	450 ± 25	1097.316	11.8 ± 0.6	0.700 ± 0.011	2.97 ± 0.10	1.97 ± 0.11	Dense
7600 ± 140	19.9 ± 0.9	150 ± 5	620 ± 5	735.728	7.7 ± 0.3	0.573 ± 0.001	1.04 ± 0.05	0.15 ± 0.06	Saturation point
8290 ± 130	18.7 ± 0.9	140 ± 5	830 ± 5	1207.349	14.0 ± 1.0	0.316 ± 0.004	0.80 ± 0.03	0.27 ± 0.04	Sparse
7820 ± 170	8.3 ± 0.5	120 ± 5	740 ± 5	973.901	9.5 ± 0.7	0.239 ± 0.001	0.384 ± 0.025	0.10 ± 0.03	Sparse
7940 ± 130	12.3 ± 0.4	130 ± 5	460 ± 5	618.751	9.0 ± 0.3	0.649 ± 0.003	1.57 ± 0.07	0.45 ± 0.08	Dense
7210 ± 130	9.3 ± 0.4	130 ± 10	360 ± 5	363.090	3.3 ± 0.9	0.015 ± 0.007	0.087 ± 0.019	0.00 ± 0.03	Sparse
7170 ± 140	15.9 ± 0.9	200 ± 5	230 ± 5	448.904	15.9 ± 1.6	0.488 ± 0.009	1.03 ± 0.09	0.45 ± 0.10	Sparse
7530 ± 120	9.0 ± 0.3	80 ± 5	550 ± 5	672.778	12.2 ± 0.7	0.420 ± 0.011	0.67 ± 0.04	0.11 ± 0.05	Sparse
7690 ± 130	32.3 ± 0.9	90 ± 5	410 ± 5	1075.366	5.5 ± 1.0	0.029 ± 0.001	0.39 ± 0.04	0.25 ± 0.04	Sparse
8060 ± 130	15.3 ± 0.7	160 ± 5	620 ± 5	907.640	17.5 ± 0.5	0.698 ± 0.001	4.06 ± 0.09	1.33 ± 0.11	Dense

Table 1. Grass parameters measured for our sample of δ Scuti stars. First and second columns are the effective temperature and luminosity by Stassun et al. (2019), respectively. The following columns are all defined in Sect. 4. Third, fourth, and fifth columns are the frequency at minimum peak density, the cut-off frequency for peak density, and the highest frequency detected, respectively. The sixth and seventh columns are the mean amplitude of the plateau, and the plateau factor, i.e., the stability of the flat plateau. The eighth and ninth columns are the mean density of peaks, and the grass density decay, respectively. Last column indicates the grass regime.

et al. 2010). Kallinger & Matthews (2010) highlight that early A stars may have a thin, but non-negligible convective layer in their surfaces. They suggest granulation as the cause of the high amount of low-amplitude peaks, including a threshold to stop the prewhitening and avoid them. However, they use a linear interpolation method that may artificially change the distribution of frequencies (Pascual-Granado et al. 2018). On the contrary, we use our non-linear interpolation method to fill the gaps achieving a significant background noise reduction (see Sect. 3). In addition, we use a local signal-to-noise ratio and, therefore, we take into account the background noise variation with frequency. Instead of only using the false alarm probability, the fractal component of the light curve should be taken into account (de Franciscis et al. 2019). The application of this technique to redefine the detection limit for the study of the grass will be the focus of future work.

In any case, our study does not rule out the granulation as a mechanism for plateau formation. One possibility may be the coupling of rotation and convection. Rotation may extend a subsurface convective zone, mainly on the equator but also at the poles (Maeder et al. 2008). Then, fast-rotating stars may have larger stochastic contributions than slow rotators. Moreover, their characteristics may change depending on the inclination from the line of sight.

5.2. Rotation, ageing, and grass regimes

As we introduced in Sect. 1 and discussed above in Sect. 5, rotation rate may be the main cause of the presence of a flat plateau. There might be not an unique mechanism related with rotation, but different flavours such as the convection - rotation connection (Maeder et al. 2008), the pulsation - rotation coupling (Buchler et al. 1995), or the emergence of chaotic modes due to the flattening of the star (e.g., Lignières & Georgeot 2009; Evano et al. 2019; Mirouh 2022). BF2017 suggested rotation rate as one of the mechanisms behind the presence of the flat plateau. In fact, they found that the higher their rotation rate, the higher their peak density. Taking into account their results, all stars at the dense grass regime should be fast rotators, and the saturation point may indicate the emergence of the chaotic modes (Barceló Forteza et al., in prep.). Furthermore, the visibility of modes in a flattened stars depends on its inclination (e.g., Reese et al. 2013, 2017), which can explain the seemingly random distribution of the mean amplitude of the flat plateau (see Fig. 12).

Age may also play a significant role. δ Scuti stars are located in the HR diagram from the main sequence to the giant branch (see Fig. 3). During the evolution process, the stellar parameters such as radius, temperature, or luminosity change with time (e.g., Pamyatnykh 2000). Therefore, the power spectra of this kind of stars also change (Breger 1998; Christensen-Dalsgaard 2000) and, consequently, their seismic indexes such as the large separation ($\Delta\nu$; e.g. García Hernández et al. 2015; García Hernández et al. 2017; Mirouh et al. 2019; Bedding et al. 2020), the frequency at maximum power ($\nu_{\rm max}$; e.g., Barceló Forteza et al. 2018, 2020; Hasanzadeh et al. 2021), or the splitting due to rotation (s; e.g., BF2017; Ramón-Ballesta et al. 2021).

Stellar rotation on the main sequence depends on the angular momentum loss and redistribution at the formation phases of the star (Sun et al. 2021). Once the initial rotation rate at the Zero-Age Main Sequence (ZAMS; $t/t_{MS} \sim 0$) has been established, the rotation evolution up to the Terminal-Age Main Sequence ($t/t_{MS} \sim 1$) can be described taking into account the physics of the star. δ Scuti stars increase their rotation rate with respect to its break-up frequency (Ω/Ω_K) from ZAMS to $t/t_{MS} \sim 0.4$ and then remain high for the rest of the main sequence (Zorec &

Royer 2012). Similarly, Georgy et al. (2013) models show an increase of the rotation rate from $t/t_{MS} \sim 0.1$ to 0.9. The higher the initial Ω/Ω_K, the greater its increase. For both cases, this growth is mainly due to the decrease of break-up frequency (Ω_K), i.e., there is a lower contribution of the gravity force against the centrifugal force.

$$\Omega/\Omega_K \propto \Omega\left(\frac{R^3}{GM}\right)^{1/2} = \sqrt{\frac{\Omega^2 R}{g_{\rm eff}}}\,. \tag{10}$$

Taking into account the Ω_K variation with age, one δ Scuti star at the sparse grass regime may increase Ω/Ω_K and, consequently, its density of peaks. Therefore, a δ Scuti star may change from a sparse grass regime to a dense grass regime, especially for these stars with intermediate to fast initial rotation close to the transition between both regimes.

6. Conclusions

The low-amplitude power spectra of δ Scuti stars contains crucial information. It can present a flat power excess known as flat plateau, or not. Both cases are of interest. This structure can be described by a high density of low-amplitude peaks between two characteristic frequencies: The frequency at minimum peak density (ν_λ), that separates the γ Doradus and δ Scuti pulsation regimes; and the cut-off frequency that is the high-frequency limit where the density of peaks drops ($\nu_{c,n}$).

The flat plateau can be quantitatively studied thanks to the low-amplitude, low-signal peaks known as grass ($\log S_i \leq -2$). There are two regimes depending on the density of these kind of peaks ($\bar{n}$) and the stability of their amplitudes (Ξ). In the sparse grass regime, the grass is not dense enough and its amplitude not uniform enough to make a flat plateau. On the contrary, in the dense grass regime, the high density of grass peaks with similar amplitude allows us to observe the flat plateau.

The saturation point ($\Xi_s \sim 0.6$) is reached at 1 grass peak per μHz, approximately. At that point, the grass density decay increases from 0.2 up to 2.75 peaks/μHz. The flat plateau is always significant in the dense grass regime, but its mean amplitude is not correlated with the density of peaks nor the plateau factor.

Unlike the grass, there are no significant differences in the high-signal peaks of the envelope ($\log S_i \geq -1$) for cases with and without flat plateau. As BF2017 suggested, the power spectra of δ Scuti stars appear to have two different structures: the envelope formed by stellar pulsations and the grass which origin still in debate.

After having parameterized the behaviour of the grass for δ Scuti stars, studying the stellar structure of each component should be mandatory. The differences between members belonging to each regime may help us to find the mechanism for the emergence of the flat plateau.

One of the most interesting candidates is rotation. The saturation point may be related to the emergence of chaotic modes due to the flattening of the star at high rotation rates. Furthermore, rotation may be related to most of the other mechanisms such as mode coupling or granulation. All these possibilities deserve to be explored by looking for rotational signatures at the power spectra such as rotational split modes or surface rotation signals.

Acknowledgements. The authors wish to thank the TESS team whose efforts made these results possible. Funding for the TESS mission is provided by the NASA Explorer Program. SBF, JCS and GMM received financial support from the Spanish State Research Agency (AEI) Projects No. PID2019-107061GB-C64: "Contribution of the UGR to the PLATO2.0 space mission. Phases C/D-1". SBF also thanks the resources received from the PLATO project collaboration with Centro de Astrobiología (PID2019-107061GB-C61). JP-G and ML-M acknowledge funding support from Spanish public funds for research under project ESP2017-87676-C5-5-R; They also acknowledge financial support from the State Agency for Research of the Spanish MCIU through the "Center of Excellence Severo Ochoa" award to the Instituto de Astrofísica de Andalucía (SEV-2017-0709). AGH acknowledges funding support from 'European Regional Development Fund/Junta de Andalucía-Consejería de Economía y Conocimiento' under project E-FQM-041-UGR18 by Universidad de Granada.

References

Antoci, V., Cunha, M., Houdek, G., et al. 2014, ApJ, 796, 118
Baglin, A., Auvergne, M., Barge, P., et al. 2006, in ESA Special Publication, Vol. 1306, ESA Special Publication, ed. M. Fridlund, A. Baglin, J. Lochard, & L. Conroy, 33
Balona, L. A. 2011, MNRAS, 415, 1691
Balona, L. A. 2014, MNRAS, 439, 3453
Balona, L. A. & Dziembowski, W. A. 2011, MNRAS, 417, 591
Barceló Forteza, S., Michel, E., Roca Cortés, T., & García, R. A. 2015, A&A, 579, A133
Barceló Forteza, S., Moya, A., Barrado, D., et al. 2020, A&A, 638, A59
Barceló Forteza, S., Roca Cortés, T., & García, R. A. 2018, A&A, 614, A46
Barceló Forteza, S., Roca Cortés, T., García Hernández, A., & García, R. A. 2017, A&A, 601, A57
Bedding, T. R., Murphy, S. J., Hey, D. R., et al. 2020, Nature, 581, 147
Borucki, W. J., Koch, D., Basri, G., et al. 2010, Science, 327, 977
Bowman, D. M. & Kurtz, D. W. 2018, MNRAS, 476, 3169
Bowman, D. M., Kurtz, D. W., Breger, M., Murphy, S. J., & Holdsworth, D. L. 2016, MNRAS, 460, 1970
Breger, M. 1998, in IAU Symposium, Vol. 185, New Eyes to See Inside the Sun and Stars, ed. F.-L. Deubner, J. Christensen-Dalsgaard, & D. Kurtz, 323
Breger, M. 2000, in Astronomical Society of the Pacific Conference Series, Vol. 210, Delta Scuti and Related Stars, ed. M. Breger & M. Montgomery, 3
Buchler, J. R., Goupil, M.-J., & Hansen, C. J. 1997, A&A, 321, 159
Buchler, J. R., Goupil, M. J., & Serre, T. 1995, A&A, 296, 405
Chevalier, C. 1971, A&A, 14, 24
Christensen-Dalsgaard, J. 2000, in Astronomical Society of the Pacific Conference Series, Vol. 210, Delta Scuti and Related Stars, ed. M. Breger & M. Montgomery, 187
de Franciscis, S., Pascual-Granado, J., Suárez, J. C., et al. 2019, MNRAS, 487, 4457
Evano, B., Lignières, F., & Georgeot, B. 2019, A&A, 631, A140
García, R. A., Mathur, S., Pires, S., et al. 2014, A&A, 568, A10
García Hernández, A., Martín-Ruiz, S., Monteiro, M. J. P. F. G., et al. 2015, ApJ, 811, L29
García Hernández, A., Suárez, J. C., Moya, A., et al. 2017, MNRAS, 471, L140
Georgy, C., Ekström, S., Granada, A., et al. 2013, A&A, 553, A24
Goode, P. R. & Thompson, M. J. 1992, ApJ, 395, 307
Harvey, J. 1985, in ESA Special Publication, Vol. 235, Future Missions in Solar, Heliospheric & Space Plasma Physics, ed. E. Rolfe & B. Battrick
Hasanzadeh, A., Safari, H., & Ghasemi, H. 2021, MNRAS, 505, 1476
Kallinger, T. & Matthews, J. M. 2010, ApJ, 711, L35
Kallinger, T., Weiss, W. W., Barban, C., et al. 2010, A&A, 509, A77
Kennelly, E. J., Brown, T. M., Kotak, R., et al. 1998, ApJ, 495, 440
Kurtz, D. W., Hubrig, S., González, J. F., van Wyk, F., & Martinez, P. 2008, MNRAS, 386, 1750
Lignières, F. & Georgeot, B. 2009, A&A, 500, 1173
Maeder, A., Georgy, C., & Meynet, G. 2008, A&A, 479, L37
Michel, E., Baglin, A., Auvergne, M., et al. 2008, Science, 322, 558
Mirouh, G. M. 2022, Frontiers in Astronomy and Space Sciences, 9, 952296
Mirouh, G. M., Angelou, G. C., Reese, D. R., & Costa, G. 2019, MNRAS, 483, L28
Moskalik, P. 1985, Acta Astron., 35, 229
Moya, A., Suárez, J. C., García Hernández, A., & Mendoza, M. A. 2017, MNRAS, 471, 2491
Murphy, S. J., Hey, D., Van Reeth, T., & Bedding, T. R. 2019, MNRAS, 485, 2380
Murphy, S. J., Shibahashi, H., & Kurtz, D. W. 2013, MNRAS, 430, 2986
Neiner, C., Wade, G. A., & Sikora, J. 2017, MNRAS, 468, L46
Pamyatnykh, A. A. 2000, in Astronomical Society of the Pacific Conference Series, Vol. 210, Delta Scuti and Related Stars, ed. M. Breger & M. Montgomery, 215
Pascual-Granado, J., Garrido, R., & Suárez, J. C. 2015, A&A, 581, A89
Pascual-Granado, J., Suárez, J. C., Garrido, R., et al. 2018, A&A, 614, A40
Poretti, E., Michel, E., Garrido, R., et al. 2009, A&A, 506, 85

Ramón-Ballesta, A., García Hernández, A., Suárez, J. C., et al. 2021, MNRAS, 505, 6217
Reese, D. R., Lignières, F., Ballot, J., et al. 2017, A&A, 601, A130
Reese, D. R., Lignières, F., Ballot, J., et al. 2013, in Astronomical Society of the Pacific Conference Series, Vol. 479, Progress in Physics of the Sun and Stars: A New Era in Helio- and Asteroseismology, ed. H. Shibahashi & A. E. Lynas-Gray, 545
Ricker, G. R., Winn, J. N., Vanderspek, R., et al. 2015, Journal of Astronomical Telescopes, Instruments, and Systems, 1, 014003
Royer, F., Zorec, J., & Gómez, A. E. 2007, A&A, 463, 671
Shibahashi, H. & Kurtz, D. W. 2012, MNRAS, 422, 738
Stassun, K. G., Oelkers, R. J., Paegert, M., et al. 2019, AJ, 158, 138
Suárez, J. C., Garrido, R., Pascual-Granado, J., et al. 2020, Frontiers in Astronomy and Space Sciences, 7, 12
Suárez, J. C., Hernández, A. G., Moya, A., et al. 2014, in IAU Symposium, Vol. 301, IAU Symposium, ed. J. A. Guzik, W. J. Chaplin, G. Handler, & A. Pigulski, 89–92
Sun, W., Duan, X.-W., Deng, L., & de Grijs, R. 2021, ApJ, 921, 145
Uytterhoeven, K., Moya, A., Grigahcène, A., et al. 2011, A&A, 534, A125
Xiong, D. R., Deng, L., Zhang, C., & Wang, K. 2016, MNRAS, 457, 3163
Zorec, J. & Royer, F. 2012, A&A, 537, A120
Zwintz, K., Neiner, C., Kochukhov, O., et al. 2020, A&A, 643, A110